

**THIOLATED ALGINATE-
POLY(LACTIC-CO-GLYCOLIC ACID)
APTAMER-FUNCTIONALISED AS A
TAMOXIFEN-CURCUMIN NANOCARRIER
AGAINST RESISTANT BREAST CANCER CELL**

CHIU HOCK ING

UNIVERSITI SAINS MALAYSIA

2023

**THIOLATED ALGINATE-
POLY(LACTIC-CO-GLYCOLIC ACID)
APTAMER-FUNCTIONALISED AS A
TAMOXIFEN-CURCUMIN NANOCARRIER
AGAINST RESISTANT BREAST CANCER CELL**

by

CHIU HOCK ING

**Thesis submitted in fulfilment of the requirements
for the degree of
Doctor of Philosophy**

December 2023

ACKNOWLEDGEMENT

I owe my heartfelt gratitude to my supervisor, Associate Professor Dr Lim Vuanghao, for his precious guidance, invaluable knowledge and utmost patience during my study. I am deeply thankful to my co-supervisors, Associate Professor Dr Md Azman Seeni Mohamed, Dr Nozlana Abdul Samad and Dr Maisarah Nasution Waras, for their helpful advice and enormous support throughout this research project.

I would also like to thank my friends and colleagues, Qiu Qiyue, Chen Zhen, Zhang Zheng, Yang Bin, Han Pengwei, Wang Fang, Batoul and Kogi for their continuous support, understanding, encouragement and technical assistance. Sincere gratitude to the Director and staff of IPPT, USM, for their technical help and support.

Thanks to the Universiti Sains Malaysia for providing the financial support (USM Fellowship Scheme) to pursue my PhD's degree, and thanks to the Ministry of Higher Education, Malaysia, for providing the Fundamental Research Grant Scheme (Reference code: FRGS/1/2018/STG07/USM/02/9, Account code: 203.CIPPT.6711684) to support this project.

Last but not least, I extend my deepest gratitude to my parents, Chiu Chow Fung and Ling Toh Ling for their constant love, selfless support, and encouragement throughout my study. Without them, this thesis would not have been possible.

TABLE OF CONTENTS

ACKNOWLEDGEMENT.....	ii
TABLE OF CONTENTS.....	iii
LIST OF TABLES	ix
LIST OF FIGURES	xiii
LIST OF SCHEMES	xviii
LIST OF SYMBOLS AND ABBREVIATIONS	xix
ABSTRAK	xxv
ABSTRACT	xxvii
CHAPTER 1 INTRODUCTION.....	1
1.1 Research Background.....	1
1.2 Problem Statements.....	5
1.3 Objective	7
CHAPTER 2 LITERATURE REVIEW.....	8
2.1 Breast Cancer	8
2.1.1 Development of Breast Cancer	9
2.1.2 Subtypes of Breast Cancer	10
2.1.3 ER-positive Breast Cancer	12
2.2 Multidrug Resistance.....	13
2.2.1 Development of MDR in Breast Cancer	14
2.2.2 ATP-Binding Cassette Superfamily	16
2.3 Nanotechnology Based Drug Delivery Systems	18
2.4 EPR Effect.....	19
2.5 Drug Targeting	20
2.5.1 Passive Targeting	21

2.5.2	Active Targeting.....	22
2.6	Polymeric Nanoparticles	23
2.6.1	Alginate-Based Nanoformulations.....	24
2.6.1(a)	Modification of Alginate	25
2.6.2	PLGA-Based Nanoformulations	27
2.7	Aptamers	32
2.7.1	AS1411 Aptamer.....	33
2.8	Tamoxifen	34
2.9	Curcumin.....	37
2.9.1	Therapeutic Activities of Curcumin.....	41
2.9.2	Chemosensitisation Effect of Curcumin	43
2.10	Apoptosis.....	44
2.11	Cell Cycle.....	48
2.12	Cellular Uptake of the Nanoparticles	50
2.12.1	Clathrin-Dependent Endocytosis.....	52
2.12.2	Caveolin-Dependent Endocytosis	52
2.12.3	Phagocytosis.....	53
2.12.4	Macropinocytosis	54
2.12.5	Clathrin and Caveolin-Independent Pathways	55
CHAPTER 3 MATERIALS AND METHODS		57
3.1	Materials.....	57
3.2	Flow of the Study	60
3.3	Development of Blank Disulfide Cross-Linked Alginate-PLGA Nanoparticles.....	62
3.4	Optimisation of TNP and CNP.....	63
3.5	Characterisations of TNP and CNP.....	64
3.5.1	Evaluation of Thiol Concentrations	64
3.5.2	ATR-FTIR Analysis.....	64

3.5.3	¹ H NMR Analysis	65
3.5.4	Particle Size and Zeta Potential.....	65
3.5.5	SEM and TEM Analyses.....	65
3.6	Preparation of Tamoxifen and Curcumin-Entrapped Alginate-PLGA Nanoparticles.....	66
3.7	Optimisation of TDL and CDL	66
3.8	Characterisations of TDL and CDL	67
3.8.1	Particle Size and Zeta Potential.....	67
3.8.2	SEM and TEM Analyses.....	67
3.8.3	Entrapment Efficiency and Entrapment Capacity	67
3.9	Development of the HPLC Method	68
3.9.1	Determination of Wavelength	68
3.9.2	Instrumentation and HPLC Conditions	68
3.9.3	Development of Standard Calibration Solutions and Corresponding Calibration Curves.....	69
3.9.4	Preparation of Quality Control Test Samples	69
3.9.5	Method Validation.....	69
3.9.5(a)	Specificity	69
3.9.5(b)	Stress Degradation Studies	70
3.9.5(c)	Linearity.....	71
3.9.5(d)	Accuracy	71
3.9.5(e)	Precision	71
3.9.5(f)	Limit of Detection and Limit of Quantification	72
3.9.5(g)	System Suitability.....	72
3.10	<i>In Vitro</i> Drug Release Studies.....	73
3.11	Preparation of AS1411 Aptamer Conjugated Blank Nanoparticles.....	73
3.12	Characterisation of ATNP and ACNP	74
3.12.1	Agarose Gel Electrophoresis.....	74

3.12.2	XPS Examination	74
3.12.3	Aptamer Conjugation Efficiency	75
3.12.4	Particle Size and Zeta Potential.....	75
3.12.5	SEM and TEM Analyses.....	75
3.13	Preparation of AS1411 Aptamer Conjugated Drugs-Entrapped Nanoparticles.....	75
3.14	Characterisations of ATDL and ACDL	76
3.14.1	Particle Size and Zeta Potential.....	76
3.14.2	SEM and TEM Analyses.....	76
3.14.3	Entrapment Efficiency and Entrapment Capacity	76
3.14.4	Aptamer Conjugation Efficiency	76
3.14.5	<i>In Vitro</i> Drug Release Studies.....	76
3.15	Accelerated Stability Studies	77
3.16	Cell Culture	78
3.17	<i>In Vitro</i> Cytotoxicity MTT Test.....	79
3.18	Cellular Uptake of ATDL and ACDL.....	79
3.18.1	Efficiency of Cellular Uptake	79
3.19	Fluorescent Microscopy Analysis	79
3.20	Confocal Laser Scanning Microscopy Analysis	80
3.21	Apoptosis Assay.....	81
3.22	Cell Cycle Analysis.....	81
3.23	HPLC Analysis of Intracellular TAM Efflux.....	82
3.24	Evaluation of P-gp Functions.....	82
3.25	Evaluation of P-gp Expression.....	83
3.26	Intracellular ATP Level Assay.....	83
3.27	Statistical Analysis	84
CHAPTER 4 RESULTS AND DISCUSSION		85
4.1	Flow of the Study	85

4.2	Evaluation of Thiol Concentrations	86
4.3	ATR-FTIR Analysis.....	89
4.4	¹ H NMR Analysis.....	93
4.5	Optimisation of TNP and CNP.....	98
4.5.1	Effect of Organic Phase: Internal Aqueous Phase Ratio.....	98
4.5.2	Effect of PVA Concentration	101
4.5.3	Effect of TSA Concentration.....	104
4.5.4	Effect of PLGA Contents	106
4.5.5	Effect of Sonication Time	108
4.5.6	Effect of Span 80 Surfactant Concentration.....	110
4.6	Development of the HPLC Method	113
4.6.1	Determination of Wavelength	113
4.6.2	Instrumentation and HPLC Conditions	113
4.6.3	Method Validation.....	114
4.6.3(a)	Specificity	114
4.6.3(b)	Stress Degradation Studies	115
4.6.3(c)	Linearity.....	117
4.6.3(d)	Accuracy	119
4.6.3(e)	Precision	120
4.6.3(f)	Limit of Detection and Limit of Quantification	120
4.6.3(g)	System Suitability	120
4.7	Optimisation of TDL and CDL	121
4.8	Entrapment Efficiency and Entrapment Capacity	126
4.9	Agarose Gel Electrophoresis.....	127
4.10	XPS Examination	131
4.11	Nanodrop UV-Vis Spectrophotometer Analysis.....	134
4.12	Particle Size and Zeta Potential.....	136

4.13	SEM and TEM Analyses.....	141
4.14	Accelerated Stability Study.....	146
4.15	<i>In Vitro</i> Drug Release Study	148
4.16	<i>In Vitro</i> Cytotoxicity MTT Test.....	154
4.16.1	MCF-7	155
4.16.2	MCF-7/TAMR-1	162
4.16.3	MCF10A	168
4.17	Efficiency of Cellular Uptake	174
4.17.1	Time-Dependent Effect.....	174
4.17.2	Dose-Dependent Effect	175
4.18	Fluorescence Microscopy Analysis.....	177
4.19	Confocal Laser Scanning Microscopy Analysis	178
4.20	Apoptosis Assay.....	181
4.21	Cell Cycle Analysis.....	184
4.22	HPLC Analysis of Intracellular TAM Efflux	187
4.23	Evaluation of P-gp Functions.....	189
4.23.1	Rh123 Accumulation and Efflux.....	189
4.24	Evaluation of P-gp Expression.....	193
4.25	Intracellular ATP Level Assay.....	195
CHAPTER 5 CONCLUSION AND FUTURE RECOMMENDATIONS....		198
5.1	Summary	198
5.2	Study Limitations	201
5.3	Recommendations for Future Research	201
REFERENCES.....		204
LIST OF PUBLICATIONS		

LIST OF TABLES

	Page
Table 2.1 Thiolated alginate derived from cysteamine hydrochloride and thioglycolic acid.	26
Table 2.2 Various methods were employed to produce PLGA nanoparticles, including emulsification evaporation, nanoprecipitation, microfluidics, and salting out.	30
Table 2.3 Various categories of regulated cell death (RCD) are currently recognised, including necroptosis, apoptosis, pyroptosis, ferroptosis and autophagy.	45
Table 3.1 Inventory of substances and compounds.	57
Table 3.2 Record of materials used for cell cultivation.	58
Table 3.3 Catalogue of apparatus and equipment.	59
Table 3.4 List of the independent factors.	63
Table 4.1 Formulation for variation in DMSO (organic phase):PVA aqueous solution (aqueous phase) ratio.	100
Table 4.2 Effect of organic phase:aqueous phase ratio on (A) TNP and (B) CNP nanoparticles (Mean±SD, n=3).	100
Table 4.3 Formulation for variation in polyvinyl alcohol (PVA) concentration.	103
Table 4.4 Effect of PVA concentration on (A) TNP and (B) CNP nanoparticles (Mean±SD, n=3).	103
Table 4.5 Formulation for variation in TSA concentration.	105
Table 4.6 Effect of TSA concentration on (A) TNP and (B) CNP nanoparticles (Mean±SD, n=3).	105
Table 4.7 Formulation for variation in PLGA contents.	107

Table 4.8	Effect of PLGA contents on (A) TNP and (B) CNP nanoparticles (Mean±SD, n=3).	107
Table 4.9	Formulation for variation in sonication time.	109
Table 4.10	Effect of sonication time on (A) TNP and (B) CNP nanoparticles (Mean±SD, n=3).	109
Table 4.11	Formulation for variation in Span 80 surfactant concentration.	112
Table 4.12	Effect of Span 80 surfactant concentration on (A) TNP and (B) CNP nanoparticles (Mean±SD, n=3).	112
Table 4.13	Tailing factor and theoretical plate numbers of CUR and TAM.	116
Table 4.14	Linearity results of CUR and TAM (Mean±SD; n=5).	119
Table 4.15	Results of accuracy for CUR and TAM (Mean±SD; n=5).	119
Table 4.16	Intra-day precision results of CUR and TAM (Mean±SD; n=5).	120
Table 4.17	Stress degradation study results of CUR and TAM (Mean±SD; n=3).	121
Table 4.18	Results of optimisation of entrapment efficiency and entrapment capacity for TDL nanoparticles (Mean±SD; n=3).	124
Table 4.19	Results of optimisation of entrapment efficiency and entrapment capacity for CDL nanoparticles (Mean±SD; n=3).	125
Table 4.20	Entrapment efficiency and entrapment capacity of CDL, TDL, ACDL and ATDL (Mean±SD; n=3).	127
Table 4.21	Conjugation efficiency of AS1411 aptamer for the nanoparticles (Mean±SD; n=3).	136
Table 4.22	Particle size, PDI, and zeta potential of ACNP, ATNP, ACDL and ATDL (Mean±SD; n=3).	138
Table 4.23	Mathematical models and parameters based on release data of (A) CUR and (B) TAM.	154
Table 4.24	IC ₅₀ doses of ACNP, ATNP, ACDL, ATDL, TAM and TAMCUR against MCF-7 cells.	159

Table 4.25	Statistical data of cell viability percentage for (A) 24 h, (B) 48 h and (C) 72 h post-treatment with ACNP, ATNP, ACDL ATDL, TAM and TAMCUR against MCF-7 cells using one-way ANOVA with post-hoc Tukey's HSD test. Data with different superscript alphabets indicate significant differences at the same dose ($p<0.05$).	160
Table 4.26	IC ₅₀ concentration of ACNP, ATNP, ACDL, ATDL, TAM and TAMCUR against MCF-7/TAMR-1 cells.	165
Table 4.27	Statistical data of cell viability percentage for (A) 24 h, (B) 48 h and (C) 72 h post-treatment with ACNP, ATNP, ACDL ATDL, TAM and TAMCUR against MCF-7/TAMR-1 cells using one-way ANOVA with post-hoc Tukey's HSD test. Data with different superscript alphabets show significant differences at the same concentration ($p<0.05$).	166
Table 4.28	IC ₅₀ values of ACNP, ATNP, ACDL, ATDL, TAM and TAMCUR against MCF10A cells.....	171
Table 4.29	Statistical data of cell viability percentage for (A) 24 h, (B) 48 h and (C) 72 h post-treatment with ACNP, ATNP, ACDL ATDL, TAM and TAMCUR against MCF10A using one-way ANOVA with post-hoc Tukey's HSD test. Data with different superscript alphabets denote significant differences ($p<0.05$) at the same dose.	172
Table 4.30	Percentage of viable, necrotic, early apoptotic and late apoptotic MCF-7/TAMR-1 cells 72 h post-treatment (Mean \pm SD, n=3). Data with different superscript letters shows significant difference ($p<0.05$) for the treatments with the same group of cells.	184
Table 4.31	Percentage of cells in G1, S and G2/M phase (mean \pm SD; n=3). Data with different superscript letters denote significant differences ($p<0.05$) between the samples within the same cell cycle phase.	187
Table 4.32	Intracellular TAM retention in MCF-7/TAMR-1 cells after 4 h treatment with ACDL and ATDL using HPLC method (Mean \pm SD,	

	n=3). ** symbol indicates significant differences ($p<0.01$) when the evaluated sample was compared to the TAM within the same group.	189
Table 4.33	The mean fluorescence intensity of Rh123 accumulation in control, TAM, TAMCUR, ACDL, ATDL and verapamil (Mean \pm SD; n=3). ** symbol shows significant differences ($p<0.01$) between the investigated sample and the TAM.....	191
Table 4.34	The mean fluorescence intensity of Rh123 efflux in control, TAM, TAMCUR, ACDL, ATDL and verapamil (Mean \pm SD; n=3). ** symbol reveals significant differences ($p<0.01$) between the assayed sample in contrast to the TAM.	193
Table 4.35	Percentage of P-gp expression in MCF-7/TAMR-1 cells 72 h post-treatment with TAM, TAMCUR, ACDL, ATDL and verapamil (Mean \pm SD; n=3). ** symbol shows significant differences ($p<0.01$) between TAM and the examined treatment.	195

LIST OF FIGURES

	Page
Figure 2.1 A variety subtypes of breast cancer. Adapted from Cilibrasi <i>et al.</i> (2021).	11
Figure 2.2 An overview of MDR activities. Adapted from Chai <i>et al.</i> (2010). ...	13
Figure 2.3 Targeting the tumour cells actively and passively assisted by the EPR effect. Adapted from Shi <i>et al.</i> (2023).	21
Figure 2.4 Structure of alginate.	24
Figure 2.5 Preparation of alginate entrapped or coated PLGA nanoparticles. Adapted from Abdelghany <i>et al.</i> (2019).	27
Figure 2.6 Structure of PLGA.	28
Figure 2.7 Chemical structure of tamoxifen.	35
Figure 2.8 Keto-enol tautomerism of curcumin.	39
Figure 2.9 Structural changes of curcumin in (A) low pH, (B) neutral and (C) increasing pH levels.	40
Figure 2.10 The apoptosis process involving the intrinsic and extrinsic pathways. Adapted from Azzwali and Azab (2019).	46
Figure 2.11 The cell cycle is regulated by CDKs, cyclins, and CDK inhibitors. Adapted from Bai <i>et al.</i> (2017).	49
Figure 2.12 Different mechanisms of cellular uptake for the nanoparticles. Adapted from Augustine <i>et al.</i> (2020).	51
Figure 3.1 Flow chart of the study.	61
Figure 4.1 The standard curves of (A) cysteamine hydrochloride and (B) thioglycolic acid (Mean±SD, n=3).	88
Figure 4.2 Thiol content of (A) CYS and CNP, and (B) TGA and TNP (Mean±SD, n=3). ** symbol shows significant difference (p<0.01) between the thiomers and nanoparticles.	89

Figure 4.3	ATR-FTIR spectra of (A) SA, (B) OSA, (C) CYS and (D) TGA. ...	91
Figure 4.4	ATR-FTIR spectra of (A) PLGA, (B) CNP and (C) TNP.	93
Figure 4.5	¹ H NMR spectra of (A) SA, (B) OSA, (C) CYS and (D) TGA.	95
Figure 4.6	¹ H NMR spectra of (A) PLGA, (B) CNP and (C) TNP.	97
Figure 4.7	UV spectra of CUR and TAM in methanol at 20 µg/mL.	113
Figure 4.8	Chromatograms of (A) solely standard CUR solution and (B) mixed standard solution of CUR and TAM at 295 nm.	114
Figure 4.9	Chromatograms of a standard solution containing 20 µg/mL of (A) CUR and (B) its mobile phase at 428 nm while (C) TAM and (D) its mobile phase at 295 nm.	115
Figure 4.10	Standard calibration curve of (A) CUR and (B) TAM (Mean±SD; n=5).	118
Figure 4.11	Agarose gel electrophoresis (2.5%; 80 kV, 40 min). Lane 1: Free AS1411 aptamer; Lane 2: ACNP; Lane 3: Mixture of CNP and free AS1411 aptamer; Lane 4: CNP. Lane 5: Free AS1411 aptamer; Lane 6: ATNP; Lane 7: Mixture of ATNP and free AS1411 aptamer; Lane 8: TNP.	131
Figure 4.12	Wide scan XPS spectra of the (A) CNP, (B) ACNP, (C) TNP and (D) ATNP.	132
Figure 4.13	N 1s signal XPS spectra of (A) CNP, (B) ACNP, (C) TNP and (D) ATNP.	134
Figure 4.14	Nanodrop 2000c spectra of AS1411 aptamer in the supernatant recovered from the experiment.	135
Figure 4.15	The distribution of particle size distribution of (A) CNP, (B) TNP, (C) CDL and (D) TDL nanoparticles based on the intensity.	139
Figure 4.16	The distribution of particle size distribution of (A) ACNP, (B) ATNP, (C) ACDL and (D) ATDL nanoparticles based on the intensity.	140
Figure 4.17	SEM micrographs of (A) CNP, (B) CDL, (C) ACNP and (D) ACDL at magnification of 50 000 × and scale bar of 1 µm.	141

Figure 4.18	SEM micrographs of (A) TNP, (B) TDL, (C) ATNP and (D) ATDL at magnification of $50\,000\times$ and scale bar of $1\,\mu\text{m}$	143
Figure 4.19	TEM micrographs of (A) CNP, (B) CDL, (C) ACNP and (D) ACDL at $10\,000\times$ magnification and scale bar of $500\,\text{nm}$	144
Figure 4.20	TEM micrographs of (A) TNP, (B) TDL, (C) ATNP and (D) ATDL at $10\,000\times$ magnification and scale bar of $500\,\text{nm}$	146
Figure 4.21	Stability studies of (A) ACDL and (B) ATDL at room temperature after regular intervals of time (Mean \pm SD, n=3).....	148
Figure 4.22	<i>In vitro</i> release profile of TAM and CUR for (A) 24 h and (B) 168 h in CDL, TDL, ACDL and ATDL (Mean \pm SD; n=3). * symbol shows that significant difference ($p<0.05$) for comparing release data between AS1411 aptamer conjugated nanoparticles and their respective unmodified nanoparticles.....	152
Figure 4.23	(A) 24 h, (B) 48 h, (C) 72 h MTT assay of MCF-7 treated with ACNP, ATNP, ACDL, ATDL, TAM, TAMCUR (Mean \pm SD, n=3). Data with the * symbol shows significant difference ($p<0.05$) compared to untreated cells.....	158
Figure 4.24	(A) 24 h, (B) 48 h, (C) 72 h MTT assay of MCF-7/TAMR-1 treated with ACNP, ATNP, ACDL, ATDL, TAM, TAMCUR (Mean \pm SD, n=3). Data with the * symbol shows significant difference ($p<0.05$) compared to untreated cells.....	165
Figure 4.25	(A) 24 h, (B) 48 h, (C) 72 h MTT assay of MCF10A treated with ACNP, ATNP, ACDL, ATDL, TAM, TAMCUR (Mean \pm SD, n=3). Data with the * symbol shows significant difference ($p<0.05$) compared to untreated cells.....	170
Figure 4.26	Cellular uptake profile of ACDL and ATDL by MCF-7/TAMR-1 cells as a function of incubation time (0.5-4 h) at IC_{50} concentrations (mean \pm SD, n=3). ** symbol indicates significant difference between the two timepoints.	175
Figure 4.27	Cellular uptake profile of ACDL and ATDL by MCF-7/TAMR-1 cells as a function of concentration ($1.6\text{-}200.0\,\mu\text{g/mL}$) over an	

	incubation period of 4 h (mean \pm SD, n = 3). * (p<0.05) and ** (p<0.01) symbols show significant difference between the two concentrations being compared.....	177
Figure 4.28	Cellular uptake of (A) ATDL and (B) ACDL by MCF-7/TAMR-1 cells (4 h) under 40 000 \times magnifications and scale bar of 40 μ m illustrated by fluorescence microscopy.....	178
Figure 4.29	Colocalisation of (red) clathrin, (green) ACDL and ATDL, (blue) nucleus, and merged confocal laser scanning microscopy photographs in MCF-7/TAMR-1 cells; scale bar of 40 μ m.....	180
Figure 4.30	Cell death effect of MCF-7/TAMR-1 cells 72 h post-treatment with (A) no treatment and staining, (B) PI/annexin-V-FITC staining without treatment, (C) TAM, (D) TAMCUR, (E) ACDL and (F) ATDL.....	183
Figure 4.31	Effects of (A) control, (B) TAM, (C) TAMCUR, (D) ACDL and (E) ATDL on the cell cycle phase of MCF-7/TAMR-1 cells. Representative cell cycle histograms showing the proportion of MCF-7/TAMR-1 cells in various phases of the cell cycle obtained by flow cytometry analysis.	186
Figure 4.32	Accumulation of Rh123 by the cells pre-treated with or without samples (A) control, (B) TAM, (C) TAMCUR, (D) ACDL, (E) ATDL and (F) verapamil.	190
Figure 4.33	Rh123 efflux study in the absence or presence of samples (A) control, (B) TAM, (C) TAMCUR, (D) ACDL, (E) ATDL and (F) verapamil.....	192
Figure 4.34	P-gp expression in MCF-7/TAMR-1 cells treated with (A) isotype control, (B) TAM, (C) TAMCUR, (D) ACDL, (E) ATDL and (F) verapamil for 72 h, and the non-specific fluorescent labelling was corrected by the isotype control.	195
Figure 4.35	Standard calibration curve of ATP standard solutions in deionised water (n=3).....	197

Figure 4.36 The ATP inhibition rate on MCF-7/TAMR-1 cells after 72 h incubation with various formulations of TAM (Mean \pm SD, n=3). ** symbol denotes significant differences (p<0.01) between the assayed treatment and TAM.....197

LIST OF SCHEMES

	Page
Scheme 3.1 Synthesis process of (A) TGA and (CYS).	62
Scheme 4.1 Schematic flow diagram for developing ACDL and ATDL nanoparticles.	86
Scheme 4.2 The reaction of Elman's reagent with thiol groups.	87
Scheme 4.3 Grafting of AS1411 aptamer to ATNP and ACNP nanoparticles via the carbodiimide reaction.	129
Scheme 4.4 MTT reduction by the mitochondrial reductase enzyme.	155

LIST OF SYMBOLS AND ABBREVIATIONS

-	Negative sign
\pm	Plus-minus sign
<	Less than
>	Greater than
\leq	Less than or equal
\geq	Greater than or equal
α	Alpha
β	Beta
π	Pi
%	Percentage
§	Section
°	Degree
°C	Degree Celsius
®	Registered trademark symbol
$\mu\text{g/mL}$	Microgram per millilitre
μL	Microlitre
μm	Micrometre
μM	Micromolar
$\times g$	Relative centrifugal force
D	D convention to chiral monosaccharides and chiral alpha-amino acids
L	L convention to chiral monosaccharides and chiral alpha-amino acids
^1H	Proton
3D	Three dimensional

ABC	ATP-binding cassette
ACD	Accidental cell death
Akt	Protein kinase B
ATP	Adenosine Triphosphate
ATR-FTIR	Attenuated total reflectance Fourier-transformed infrared spectroscopy
ANOVA	One-way analysis of variance
BSA	Bovine serum albumin
CDK	Cyclin-dependent kinase
cm	Centimetre
cm ⁻¹	Reciprocal centimetre
CO ₂	Carbon dioxide
CUR	Curcumin
CYP	Cytochrome P450
D ₂ O	Deuterium oxide
DAD	Diode array detector
DAPI	4',6-diamidino-2-phenylindole
DLS	Dynamic light scattering
DMEM	Dulbecco's modified eagle medium
DMSO	Dimethyl sulfoxide
DNA	Deoxyribonucleic acid
DOX	Doxorubicin
DTNB ²⁻	5,5'-dithiobis(2-nitrobenzoic acid)
EAM	European Association of Medicine
EDAC	1-(3-dimethylaminopropyl)-3-ethylcarbodiimide hydrochloride
EPR	Enhanced permeability and retention
ER	Oestrogen receptor

eV	Electron-volts
FACS	Fluorescence-activated cell sorting
FDA	Food and Drug Administration
FTIR	Fourier transform infrared spectroscopy
g	Gram
g/mol	Gram per mole
GA	Glycolic acid
GFR	Growth factor receptor
GRAS	Generally recognised as safe
GSH	Glutathione
G block	α -l-guluronic acid
G phase	Growth phase
h	Hour
H ₂ O	Water
HeLa	Human cervical cancer cell line
HepG2	Human hepatocellular carcinoma cell line
HER2	Human epidermal growth factor receptor-2 oncogene
HLB	Hydrophilic–lipophilic balance
HPLC	High performance liquid chromatography
HSD	Honestly Significant Difference
IC ₅₀	Specific half maximal inhibitory concentration
ICH	International Conference on Harmonisation of Technical Requirements for Registration of Pharmaceuticals for Human Use
K562	Human leukemic cell line
kV	Kilovolt
LA	Lactic acid
LC/MS	Liquid chromatography-mass spectrometry

LC-MS/MS	Liquid chromatography-tandem mass spectrometry
LOD	Limit of detection
LOQ	Limit of quantification
M	Molarity
m	Metre
MAPK	RAS/RAF/mitogen-activated protein kinase
MCF-7	Human breast cancer cell line
MCF-7/TAMR-1	Tamoxifen-resistant MCF-7 cell line
MCF10A	Normal human mammary epithelial cells
MDR	Multidrug resistance
MES	2-(N-morpholino)ethanesulfonic acid
mg	Milligrams
mg/mL	Milligram per millilitre
MHz	Megahertz
min	Minute
mL	Millilitre
mM	Millimolar
MTBE	Methyl-tert-butyl ether
mTOR	Mammalian target of rapamycin
MTT	3-(4,5-dimethylthiazol-2-yl)-2,5-diphenyltetrazolium bromide
mV	Millivolt
M block	β -d-mannuronic acid
M phase	Mitotic phase
n	Number of replicates
NaOD	Sodium deuterioxide
NaOH	Sodium hydroxide
NF- κ B	Nuclear factor kappaB

NHS	N-hydroxysuccinimide
nm	Nanometre
NMR	Nuclear magnetic resonance
P-gp	P-glycoprotein
PARP	Poly(ADP-ribose) polymerase
PBS	Phosphate buffer saline
PDI	Polydispersity index
PEG	Polyethylene glycol
PFA	Paraformaldehyde
PI	Propidium iodide
PI3K	Phosphoinositide 3-kinase
PLA	Polylactic acid
PLGA	Poly(lactic-co-glycolic acid)
ppm	Parts per million
PR	Progesterone receptor
PS	Phosphatidylserine
PTA	Phosphotungstic acid
PTFE	Polytetrafluoroethylene
PVA	Polyvinyl alcohol
R ²	Coefficient of determination
RAF	Rapidly accelerated fibrosarcoma
RAS	Rat sarcoma
RCD	Regulated cell death
RE	Relative error
RES	Reticuloendothelial system
Rh123	Rhodamine 123
rRNA	Ribosomal RNA

ROS	Reactive oxygen species
rpm	Revolutions per minute
RPMI	Roswell Park Memorial Institute 1640
RSD	Relative standard deviation
RT-PCR	Reverse transcription polymerase chain reaction
SD	Standard deviation
SDS	Dodecyl sulphate sodium salt
SELEX	Systematic Evolution of Ligands by Exponential Enrichment
SEM	Scanning electron microscopy
SERD	Selective oestrogen receptor downregulator
SERM	Selective oestrogen receptor modulation drug
ssDNA	Single-stranded DNA
TAE	Tris-acetate-EDTA
TAM	Tamoxifen
TEM	Transmission electron microscopy
USP	US Pharmacopeia
UV	Ultraviolet
Vis	Visible
w/v	Weight per volume
XPS	X-ray photoelectron spectroscopy

**ALGINAT-POLI(ASID LAKTIK-KO-GLIKOLIK) TERTIOL
BERFUNGSIKAN APTAMER SEBAGAI NANOPEMBAWA TAMOSIFEN-
KURKUMIN TERHADAP SEL KANSER PAYUDARA TERINTANG**

ABSTRAK

Terapi kanser payudara sering gagal disebabkan oleh perkembangan rintangan pelbagai drug (MDR), yang biasanya dimediasi oleh ekspresi berlebihan P-glikoprotein (P-gp), iaitu pengangkut efluks drug yang hadir dalam membran. Kaedah penyampaian drug secara tradisional bagi kemoterapi drug tunggal mempunyai batasan seperti bioavailabiliti yang rendah, pelepasan yang cepat, dan MDR. Gabungan kemoterapi telah mengurangkan MDR dan kesan sampingannya, tetapi isu ketoksikan kekal sebagai cabaran. Sistem penghantaran drug yang disasarkan telah dibangunkan untuk mengatasi rintangan drug dan meningkatkan keberkesanan dan keselamatan terapi kanser. Sistem ini lebih selamat daripada terapi konvensional dan membenarkan dos-dos drug yang lebih tinggi, yakni penting untuk meningkatkan keberkesanan dan mengurangkan ketoksikan. Objektif projek ini ialah untuk merekabentuk nanopartikel alginat tertiol dengan fabrikasi permukaan poli(asid laktik-ko-glikolik) (PLGA) dan aptamer AS1411 untuk penghantaran sasaran tamosifen (TAM) dan kurkumin (CUR) kepada sel-sel kanser payudara yang terintang. Nanopartikel alginat tertiol telah disediakan melalui proses swa-pasangan dan disalut dengan PLGA untuk biofungsi dan lapisan perlindungan drug. TAM dan CUR telah terperangkap ke dalam nanopartikel alginate tertiol-PLGA yang berfungsi aptamer AS1411 (ACDL dan ATDL). Nanopartikel ACDL dan ATDL menunjukkan saiz partikel <280 nm dengan nilai PDI <0.35 dan potensi zeta >-16 mV, menunjukkan partikel bersaiz nano yang stabil dengan taburan saiz sempit. Ekoran ini, kecekapan

pemerangkapan TAM dan CUR dalam nanopartikel ACDL dan ATDL ialah masing-masing $\sim 40\%$ dan $<10\%$, menunjukkan bahawa pemerangkapan bersama TAM dan CUR dalam nanopartikel ACDL dan ATDL berjaya. Kecekapan konjugasi aptamer AS1411 direkodkan sebagai $> 26\%$, menyediakan sasaran kanser untuk nanopartikel. Pelepasan kumulatif CUR ($> 44\%$) dan TAM ($> 65\%$) mencapai dataran pada 72 jam dalam nanopartikel ACDL dan ATDL, menunjukkan nanopartikel ACDL dan ATDL mempamerkan pelepasan ubat yang berterusan. Kajian *in vitro* dilakukan dengan menggunakan sel-sel MCF-7, MCF-7/TAMR-1, dan MCF-7/10A. Kebolehidupan sel MCF-7/TAMR-1 jauh lebih rendah ($p<0.05$) daripada sel MCF-7/10A selepas 72 jam rawatan dengan nanopartikel ACDL dan ATDL, membuktikan nanopartikel adalah selektif terhadap sel kanser berbanding sel normal. Nanopartikel ACDL dan ATDL juga mendorong apoptosis awal dan penahanan kitaran sel pada fasa G0/G1 dalam sel MCF-7/TAMR-1, menunjukkan bahawa nanopartikel berkesan dalam menyekat pertumbuhan sel kanser payudara terintang. Pengambilan selular nanopartikel ACDL dan ATDL menunjukkan keputusan yang bergantung pada masa dan dos, dengan pengeraman dan kepekatan optimum selama 2 jam serendah $6.3 \mu\text{g/mL}$ melalui endositosis pengantara reseptor nukleolin dan klathrin. Nanopartikel ACDL dan ATDL menindas ekspresi P-gp dan aktiviti ATP sambil meningkatkan pengumpulan dan pengekalan tamosifen intraselular. Kesimpulannya, keputusan menunjukkan bahawa nanopartikel ACDL dan ATDL berpotensi menjadi agen antikanser yang berkesan untuk terapi kanser payudara terintang dengan meningkatkan pengekalan drug dan mengurangkan ekspresi P-gp dan aktiviti ATP.

**THIOLATED ALGINATE-POLY(LACTIC-CO-GLYCOLIC ACID)
APTAMER-FUNCTIONALISED AS A TAMOXIFEN-CURCUMIN
NANOCARRIER AGAINST RESISTANT BREAST CANCER CELL**

ABSTRACT

Breast cancer therapy often fails due to the development of multidrug resistance (MDR), which is commonly mediated by the overexpression of P-glycoprotein (P-gp), a drug efflux transporter presents in the membrane. Traditional drug delivery methods for single-drug chemotherapy have limitations such as low bioavailability, fast clearance, and MDR. Combination chemotherapy has reduced MDR and side effects, but toxicity issues remain a challenge. Targeted drug delivery systems have been developed to overcome drug resistance and improve cancer therapy effectiveness and safety. These systems are safer than conventional therapies and allow for greater drug doses, which is essential for improving efficacy and reducing toxicity. The objective of this project is to create thiolated alginate nanoparticles with the surface fabrication of poly(lactic-co-glycolic acid) (PLGA) and AS1411 aptamer for targeted delivery of tamoxifen (TAM) and curcumin (CUR) to resistant breast cancer cells. The thiolated alginate nanoparticles were prepared under the self-assembly process and further coated with PLGA for biofunctionalisation and a drug protection layer. TAM and CUR were entrapped into AS1411 aptamer and PLGA fabricated thiolated alginate nanoparticles (ACDL and ATDL). ACDL and ATDL nanoparticles showed particle sizes of <280 nm with PDI values <0.35 and zeta potential of >-16 mV, showing stable nano-sized particles with narrow size distribution. Herein, the entrapment efficiencies of TAM and CUR in ACDL and ATDL nanoparticles were ~40% and <10%, respectively, indicating that the co-entrapment of TAM and CUR in

the ACDL and ATDL nanoparticles was successful. The conjugation efficiency of AS1411 aptamer was recorded as >26%, providing cancer targeting for the nanoparticles. The cumulative release of CUR (>44%) and TAM (>65%) reached a plateau at 72 h in ACDL and ATDL nanoparticles, indicating that the ACDL and ATDL nanoparticles exhibited sustained drug release. *In vitro* studies were performed using MCF-7, MCF-7/TAMR-1, and MCF-7/10A cells. The viability of MCF-7/TAMR-1 cells was significantly lower ($p<0.05$) than MCF-7/10A cells 72 h post-treatment with ACDL and ATDL nanoparticles, proving that the nanoparticles were selective against cancer cells over normal cells. ACDL and ATDL nanoparticles also induced early apoptosis and cell cycle arrest at the G0/G1 phase in MCF-7/TAMR-1 cells, showing that the nanoparticles were effectively suppressed the growth of resistant breast cancer cells. The cellular uptake of ACDL and ATDL nanoparticles showed time- and dose-dependent results, with an optimum 2 h incubation and concentration as low as 6.3 $\mu\text{g/mL}$ via nucleolin receptor- and clathrin-mediated endocytosis. ACDL and ATDL nanoparticles suppressed P-gp expression and ATP activity while improving intracellular tamoxifen accumulation and retention. In conclusion, the results suggest that ACDL and ATDL nanoparticles have the potential to be effective anticancer agents for resistant breast cancer therapy by improving drug retention and reducing P-gp expression and ATP activity

CHAPTER 1

INTRODUCTION

1.1 Research Background

Drug resistance is a major cause of therapeutic failure in treating several cancers, including breast cancer (MacDonagh *et al.*, 2015). Clinical drug resistance is caused by a variety of mechanisms, including noncellular and cellular mechanisms. The conventional type of multidrug resistance (MDR), which is generally mediated by the overexpression of P-glycoprotein (P-gp) and other membrane transporters, is one of the most studied cellular mechanisms (Kartal-Yandim *et al.*, 2016). P-gp is a drug efflux transporter in the membrane that decreases intracellular levels of various structurally unrelated drugs (Vahedi *et al.*, 2017), such as tamoxifen, a cytotoxic anticancer drug frequently used in breast cancer treatment regimens (Kastrati *et al.*, 2021). This transporter has been discovered in 63% of patients with untreated breast cancer (Wang *et al.*, 2011). Decreased clinical response rates have also been linked to increased P-gp expression in breast cancer after chemotherapy (Vishnukumar *et al.*, 2013). New drug delivery technologies, such as nanoparticles, have been investigated to overcome drug resistance and increase the efficacy and safety of cancer treatment (Baek & Cho, 2017). Compared to conventional drug therapy, nanodrug delivery systems mostly exhibit reduced toxicity, allowing higher drug dosages to be safely delivered. This reduced toxicity is clinically significant since many cytotoxic agents display poor therapeutic indices.

In the treatment of breast cancer cells particularly oestrogen receptor (ER)-positive MCF-7 cell line, tamoxifen is the most commonly used anti-oestrogen, but resistance remains an obstacle in the treatment of hormone-dependent breast cancer.

Entrapped formulations of cytotoxic drugs and compounds with P-gp inhibitory action have been investigated to treat drug-resistant cancer (Da Silva *et al.*, 2017). Among these formulations, nanodrug carriers entrapped with curcumin have shown particularly effective in overcoming MDR phenotypes. Curcumin may decrease P-gp and cytochrome P450 3A4 enzyme activity, reducing tamoxifen's first-pass metabolism (Cho *et al.*, 2012). Therefore, in this study, tamoxifen and curcumin were chosen as the drug excipients to treat and sensitise tamoxifen resistant breast cancer cells MCF-7/TAMR-1. Some nanodrug carriers might be designed to stay longer in circulation or to produce larger tumoral drug concentrations with less toxicity and pharmacokinetic interactions than free drugs (Kumari *et al.*, 2016). Nanoparticles have long been known for carrying drugs across the P-gp-rich blood-brain barrier without compromising their structural integrity (Tang *et al.*, 2016). There have also been reports of anticancer drugs having increased cytotoxicity against drug-resistant cancer cells when incorporated into polymeric nanoparticulate systems (Yang *et al.*, 2016).

Polymeric nanoparticles are drug carriers with an enormous promise to enhance MDR cancer treatment. Polymeric nanoparticles offer excellent physicochemical properties, minimal intrinsic toxicity toward noncancerous tissues, surface-engineered potential, and controllable burst effect problems (Prabhu *et al.*, 2015). Although gradual drug release may result in decreased systemic toxicity, long-term exposure to low doses of cytotoxic drugs may cause P-gp overexpression (Avnet *et al.*, 2016), making cancer cells more drug-resistant. Furthermore, because of the increased efflux, MDR cells need greater drug dosages to be killed than non-resistant cells. A formulation with increased drug release rates may be preferable in this case.

Alginate is a naturally occurring anionic polymer derived from brown seaweed that has been intensively explored recently. Due to its biocompatibility, bioadhesives and biodegradability, alginate is employed in numerous biomedical applications (Hamed *et al.*, 2016). The porosity of alginate makes it a promising excipient for the entrapment and stabilisation of hydrophobic anticancer drugs (Ibrahim *et al.*, 2020). The swelling of alginate acts as a diffusion barrier which exerts drug release slowly, allowing a controlled release mechanism. The prolonged release of the drug at the target site can enhance the bioavailability of the drug. Abundant hydroxyl groups and carboxyl groups present in the backbone of the alginate chain provide a site for the conjugation thiol-bearing group. The formation of alginate-based nanoparticles is facile. For instance, disulfide cross-linked nanoparticles are readily generated by self-assembling the thiolated alginate chains (Gao *et al.*, 2017).

The surface of the nanoparticles was coated with poly(lactic-co-glycolic acid) (PLGA) after the generation of disulfide cross-linked nanoparticles. This surface fabrication acts as a controlled release mechanism. Because of its biocompatibility and biodegradability, PLGA is suitable for surface functionalisation (Rafiei & Haddadi, 2017). Furthermore, it is widely regarded as safe by the US Food and Drug Administration (FDA) (Colzani *et al.*, 2018). Significant research has been conducted on developing PLGA assemblies as a controlled release and drug entrapment technique (Wanawananon *et al.*, 2016). However, none of these investigations probed into the direct conjugation of PLGA layers onto disulfide cross-linked sodium alginate nanoparticles.

The AS1411 aptamer is an excellent breast cancer cell targeting ligand. AS1411 aptamer is a G-rich quadruplex-forming oligodeoxynucleotide that binds to

nucleolin, a protein present on the surface and in the cytoplasm of most cancer cells but not on the surface or in the cytoplasm of most normal cells (Reyes-Reyes *et al.*, 2015). AS1411 aptamer has shown potential therapeutic efficacy and is extensively utilised as a tumour-targeting ligand that may selectively target a range of attached molecules or nanomaterials to tumour cells (Baeza *et al.*, 2015). AS1411 aptamer has already entered Phase II clinical trials to treat acute myeloid leukaemia. The findings showed that coupling AS1411 aptamer with cytarabine may improve anti-leukemic activity while maintaining an acceptable patient safety profile (Li *et al.*, 2015). As a result, AS1411 aptamer alteration on nanoparticles would promote selective localisation by tumour cells and subsequent endocytosis through the interaction of AS1411 aptamer with nucleolin.

The engineering of targeting nanocarriers that entrapped a high load of multiple anticancer drugs for controlled release via surface modification of these nanocarriers with tumour targeting ligands that would facilitate local drug accumulation, enhance drug bioavailability, and prolong systemic circulation is critical to achieving this goal. As a result, this work evaluated the targeted co-delivery of tamoxifen and curcumin to resistant breast cancer cells employing self-assembly PLGA-alginate nanoparticles with AS1411 aptamer as a targeting ligand conjugated to the outer layer of PLGA. The cytotoxicity mechanism, cellular uptake, and potential ability to reverse MDR were studied.

1.2 Problem Statements

Traditional nanocarrier drug delivery methods have significant drawbacks regarding the systemic administration of single-drug chemotherapy, including quick blood/renal clearance, low bioavailability, and MDR (Zhang *et al.*, 2016). Although combination chemotherapy using numerous anticancer drugs has been introduced to decrease MDR and side effects, achieving a strong antitumour effect while minimising tissue toxicity remains difficult (Mokhtari *et al.*, 2017). Due to nanocarriers' limited entrapment capacity, several injections are required to obtain an optimal therapeutic impact, which might result in systemic toxicity and a severe inflammatory response (Zheng *et al.*, 2022).

The efficacy of conventional drug therapy in resistant-breast cancer cells is low due to the MDR effect. Overexpression of P-gp and MDR-related transport proteins is the main reason for the low efficacy of chemotherapy in resistant-breast cancer cells (Karthika *et al.*, 2022). The chemotherapeutic drugs are actively transported out from resistant-breast cancer by the P-gp mechanism. Therefore, resistant-breast cancer cells are harder to suppress by chemotherapeutic agents' cytotoxic action than non-resistant breast cancer cells. The recurrence of breast cancer incidence is often related to the MDR effect (Gote *et al.*, 2021).

In addition, the low solubility, biodistribution and bioavailability of chemotherapeutic drugs are the reason for the poor performance in chemotherapy (Lorscheider *et al.*, 2021). The anticancer agents are often metabolised and eliminated before reaching the target site. Chemotherapeutic agents cannot differentiate between normal and cancer cells. Toxicity in normal cells can cause severe side effects for the

chemotherapy subject (Mortezaee *et al.*, 2019). Therefore, nanocarriers coupled with cancer-targeting properties and controlled release mechanisms are desirable.

1.3 Objective

The main objective of this study is to develop novel biodegradable thiolated sodium alginate derivative nanoparticles with the surface fabrication of PLGA and conjugated with AS1411 aptamer for targeted delivery of tamoxifen-curcumin to resistant breast cancer cells.

The sub-objectives are:

1. To synthesise thiolated sodium alginate derivative biodegradable polymers based on thioglycolic acid and cysteamine hydrochloride.
2. To characterise thiolated alginate derivative nanoparticles layer of PLGA and functionalise a tumour specific ligand, AS1411 aptamer.
3. To characterise the aptamer conjugated tamoxifen-curcumin entrapped nanoparticles.
4. To analyse drug release profile, cellular uptake, and specific internalisation from the formulated nanoparticles in resistant breast cancer cells.
5. To elucidate the underlying mechanism of cytotoxicity and drug efflux (MDR) of the dual drug entrapped nanoparticles in resistant breast cancer cells.

CHAPTER 2

LITERATURE REVIEW

2.1 Breast Cancer

Despite the various health indicators showing an improving quality of life, cancer remains one of the primary reasons for fatalities worldwide. In 2022, an estimated 1.9 million new cancer cases and 609,360 deaths are anticipated in the United States, with breast cancer persisting as the most prevalent type at 287,850 annual cases (Siegel *et al.*, 2023). Globally, approximately 19.3 million new cancer cases were detected in 2020, and there is an anticipation that the number of cases will keep increasing by 47% by 2040 (Sung *et al.*, 2021). In 2020, the incidence of breast cancer exceeded that of lung cancer in terms of new cases. It is regarded as the most common cancer among women globally (Farghadani & Naidu, 2022). In 2020, breast cancer had the highest number of newly diagnosed cancer cases in Malaysia, representing 17.3% or 8418 cases, and accounted for 11.9% or 3503 of the total cancer deaths in the country (Azizah *et al.*, 2015; Lim & Yusuf, 2022). Breast cancer is recognised as the dominant form of cancer among women across the globe. It accounts for about 25% of all malignancies in developed nations. It is also considered a significant factor in cancer-related fatalities among females globally (Liu & Chen, 2013).

Breast cancer has five stages, from Stage 0, characterised as carcinoma *in situ*. In Stage I of breast cancer, the tumour size is less than 2 cm, and there is no lymph invasion, whereas Stage II involves lymph invasion and a tumour size ranging from 2-5 cm. Breast cancer at Stage III is identified by the presence of a tumour larger than 5 cm and lymph invasion. On the other hand, when cancer cells spread to other organs,

it is considered Stage IV, the most advanced stage of breast cancer. As the stages of breast cancer progress, the survival rate decreases. Stage I has a survival rate of over 95%, Stage III has a survival rate of around 70%, and Stage IV has a survival rate of approximately 25% (Liu & Ho, 2018).

Approximately 70% of breast cancers exhibit positive oestrogen receptor (ER) status, and antioestrogen therapy can be employed for their treatment (Masuda *et al.*, 2012). Breast cancer is known to be caused by genetic mutations in *BRCA1* and *BRCA2* (Das *et al.*, 2010). In order to treat breast cancer, various treatment methods have been used. These include surgery, radiation therapy, targeted therapy, and endocrine therapy (Harbeck *et al.*, 2019). Currently, the predominant approach for treating different forms of cancer is chemotherapy. However, this method can also cause harm to healthy cells.

2.1.1 Development of Breast Cancer

Hormonal factors, which are recognised to be associated with the onset of breast cancer, may influence the behaviour of breast cancer cells. About a third of these tumours are sensitive to endocrine therapy. Despite its beneficial effects, oestrogen has been associated with an increased risk of developing breast cancer. Oestrogen exposure in human is a risk factor that increases development of breast cancer with prolonged use and continuous doses. An association has been observed between the development of breast cancer and the level of oestrogen in the body, with higher levels of circulating oestrogen known to increase the risk of breast cancer (Toniolo *et al.*, 1995; Feigelson *et al.*, 1996; Calaf, 2014). The presence of oxidative stress is considered one of the primary factors that can contribute to cancer development. The nuclear factor kappaB (NF-κB) complex, which regulates growth and facilitates the

transition from G0 to S-phase, has been shown to enable cancer cells to resist treatment (Calaf, 2014; Mortezaee *et al.*, 2019).

The progression of breast cancer can be impacted by several factors, such as genetic susceptibility and oestrogen levels, which can alter the signalling pathways and affect the cell cycle (Hu *et al.*, 2018). The cyclin-dependent kinases (CDKs), phosphoinositide 3-kinase (PI3K)/protein kinase B (Akt)/mammalian target of rapamycin (mTOR), rat sarcoma (RAS)/rapidly accelerated fibrosarcoma (RAF)/mitogen-activated protein kinase (MAPK) and ER are among the signalling pathways involved in breast cancer progression (Arnedos *et al.*, 2015; Hart *et al.*, 2015).

2.1.2 Subtypes of Breast Cancer

The main factor that influences the development of breast cancer subtypes is the alteration or deficiency of specific hormone and growth factor receptors, including but not limited to the ER, progesterone receptor (PR), and human epidermal growth factor receptor 2 (HER2) oncogene (Holliday & Speirs, 2011; Dai *et al.*, 2016) (Figure 2.1).

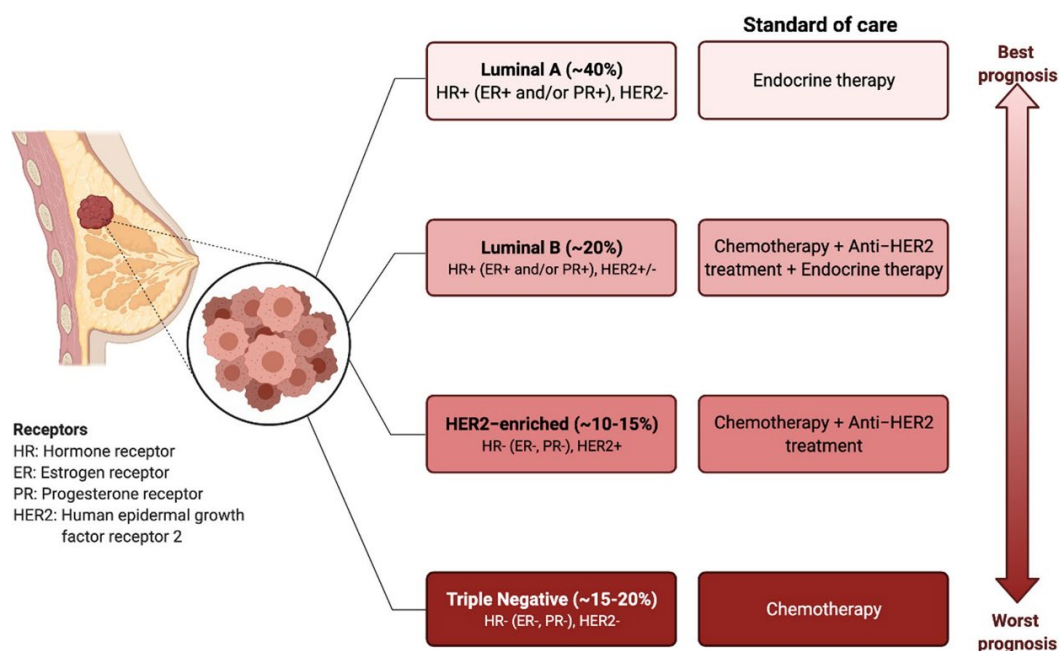


Figure 2.1: A variety subtypes of breast cancer. Adapted from Cilibrasi *et al.* (2021).

ER-positive and PR-positive are hormone-sensitive forms of breast cancer responsive to treatment with aromatase inhibitors, selective ER antagonists, and other therapies (Fan *et al.*, 2015; Lim *et al.*, 2016). Breast tumours of the luminal type seem to originate from the luminal cells inside the mammary duct (Clarke *et al.*, 2015). Luminal A breast cancer is categorised as cases with strong positive results for ER and PR. In contrast, cases with weak positive results for ER and PR are categorised as luminal B breast cancer (Tang *et al.*, 2016). Luminal A breast cancer has high cure rates and responds well to hormone therapy but poorly to chemotherapy. Hormone therapy can be a treatment option for luminal B breast cancer, although some subgroups may be harder to treat due to gene mutations. The standard approach for treating luminal B breast cancer is chemotherapy. It shows a good therapeutic response, but hormone therapy requires more control than luminal A due to higher gene expression variation (Liu & Ho, 2018).

HER2-positive breast cancer is a type of breast cancer that is negative for hormone receptors but positive for human epidermal growth factor receptor 2. HER2

overexpression is associated with poor prognosis and an aggressive disorder (Sinha *et al.*, 2012; Goel *et al.*, 2016). Although there has been a notable increase in the survival rate of patients with this type of cancer who are not responsive to hormones, the adverse effects associated with targeted therapies remain a significant obstacle (Iqbal & Iqbal, 2014; O'Sullivan & Smith, 2014; Sodergren *et al.*, 2016). Triple-negative breast cancer is identified by the lack of expression of PR and ER and is classified as a basal-like subtype of breast cancer. They are commonly known as "basal-like" because they primarily develop in the basal cells of the mammary ducts (Clarke *et al.*, 2015). It also lacks the overexpression of HER2. The triple-negative breast cancer subtype is characterised by its aggressive nature, linked to its high rate of relapses and frequent lung and brain metastasis (Bianchini *et al.*, 2016; Bimonte *et al.*, 2020).

2.1.3 ER-positive Breast Cancer

ERs are a type of transcription factor regulated by ligands and are responsible for translating hormone signals into a diverse range of physiological responses across multiple organs (Saha *et al.*, 2019). ER α and ER β , which are closely related in structure, are produced by distinct genes and exhibit varying expression levels in different tissues. ER α is responsible for transmitting the signal for oestrogen-induced cell growth in breast, uterine, and ovarian tissue epithelial cells (Pedram *et al.*, 2014). ER α and ER β are vital in controlling the growth and specialisation of cells in the normal mammary gland through their interaction with oestradiol (Renoir *et al.*, 2013). In normal breast tissue, the expression levels of ER isoforms are comparably low, but in breast cancer cells, ER α is expressed more than ER β , making it the dominant form (Huang *et al.*, 2014).

The MCF-7 cell line's significant contribution to breast cancer research lies in its usefulness for studying the ER α . It mimics the ER expression in most invasive

human breast cancers, making it an essential model for research (Lee *et al.*, 2015). MCF-7, classified under the luminal A molecular subtype, has been identified as ER-positive and PR-positive (Comşa *et al.*, 2015). Despite being a non-invasive and poorly aggressive cell line, it is commonly regarded as having low metastatic potential (Gest *et al.*, 2013).

2.2 Multidrug Resistance

Multidrug resistance (MDR) often limits the efficacy of chemotherapy, which is a frequently employed method for treating cancer (Figure 2.2). MDR in cancer cells occurs through various mechanisms, including reduced drug intake, lower intracellular drug levels, modified cell cycle checkpoints, changes in drug targets, enhanced drug metabolism, and activation of genes hindering the natural cell elimination process.

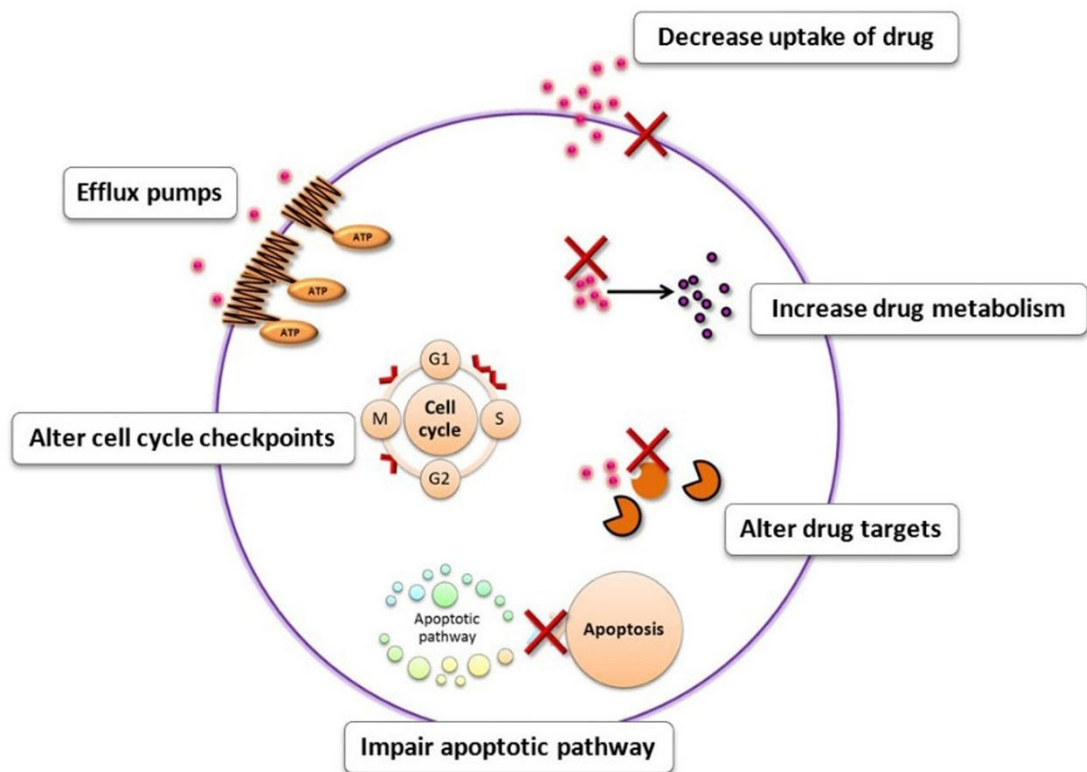


Figure 2.2: An overview of MDR activities. Adapted from Chai *et al.* (2010).

Chemotherapy-associated drug resistance can be categorised into two categories: acquired and intrinsic. The intrinsic mode, which encompasses factors pre-established in the cancer cells' microenvironment, can potentially induce the emergence of resistance (Das *et al.*, 2010). On the other hand, acquired resistance can develop in cancer cells that are sensitive or mutation prone. The development of acquired resistance in cancer cells can be caused by various factors, such as the stimulation of the cancer-promoting pathway or the over-expression of specific therapeutic targets (Sa & Das, 2008). Although chemotherapy mainly focuses on killing cancer cells, it can also affect healthy ones. The effect of chemotherapy on healthy cells can cause severe side effects, leading to organ dysfunction (Das *et al.*, 2010; Panda *et al.*, 2017). Other common side effects of chemotherapy include pain, fatigue, and infection. In addition to cancer cells, other types of tissues and organs, such as hair follicles, hematopoietic cells, and normal haematocrits, are also affected by prolonged exposure to drugs for treating cancer (Panda *et al.*, 2017). Unfortunately, this treatment often fails in some conditions due to side effects caused by drug resistance and the toxicity of the drugs (Aggarwal, 2004).

2.2.1 Development of MDR in Breast Cancer

Breast tumours may exhibit two distinct forms of resistance to first-line endocrine therapies. *De novo* resistance, characterised by the lack of response to treatment from the outset, is observed in certain tumours. The second is acquired resistance, which occurs when tumours initially respond well but later regrows or recur (Clarke *et al.*, 2015). ER is a hormone-activated transcription factor that regulates endocrine response and cell cycle genes (Yoon *et al.*, 2013). Tamoxifen inhibits the conventional ER transcriptional program, but in tamoxifen-resistant breast cancer, ER is still recruited to chromatin in new regions associated with poor outcomes, leading

to tumour progression and tamoxifen resistance (Ross-Innes *et al.*, 2012; Xue *et al.*, 2016).

Tamoxifen resistance may occur due to alterations in specific transcription factors that are linked to the ER (Schiff *et al.*, 2000; Yde *et al.*, 2012). Furthermore, resistance to chemotherapy may result from the activation of cellular signalling pathways that enhance cell susceptibility, as well as the downstream regulation of proteins that regulate cell cycle and apoptosis (Steelman *et al.*, 2011; Vallabhaneni *et al.*, 2011; Larsen *et al.*, 2012; Jiang *et al.*, 2013). It has been known that a single molecule cannot prevent negative feedback loops and crosstalk in cellular networks. As a result, the development of multi-target drugs has been regarded as the new trend in the fight against resistant breast cancer (Jiang *et al.*, 2013).

Several ways in which cancer cells can become resistant to tamoxifen have been documented, such as the interaction between ER and growth factor receptors (GFRs), mutations or loss of ER (Lee *et al.*, 2015), elevated levels of antioestrogen binding sites, and the participation of micro ribonucleic acid (miRNA) abnormalities (Wei *et al.*, 2014), changes in ER signalling and GFR network, reduced ER expression, increased expression of certain GFRs, PI3K/Akt/mTOR pathway activation (Hosford & Miller, 2014), and induction of NF- κ B signalling, which is associated with the development of ER-positive breast cancer and inability to respond to endocrine therapy (Gil, 2014). In addition, cells can develop resistance by decreasing the levels of active 4-hydroxytamoxifen through an altered metabolism of tamoxifen (Nass & Kalinski, 2015). Moreover, tumour evolution and tamoxifen resistance can be attributed to breast cancer stem cells (Droog *et al.*, 2013).

The resistance to endocrine therapy emerges from a combination of genetic alterations (sequence modifications in the deoxyribonucleic acid (DNA)) and epigenetic modifications (inheritable alterations in the activity of genes) (Bianco & Gévry, 2012; Nass & Kalinski, 2015). Several cellular alterations have been proposed to be linked with the development of acquired insensitivity to anti-oestrogenic treatment (Thomas *et al.*, 2013). One possible cause of acquired resistance to antioestrogen medications could be mutations in the gene encoding ER or its regulators (Li *et al.*, 2013; Robinson *et al.*, 2013). Genetic mutations can induce a conformational change in the ligand binding domain of ER, reducing its affinity for the medication tamoxifen. As a result, tamoxifen becomes ineffective in treating the illness. Furthermore, this alteration in conformation also leads to cell proliferation and tumour advancement, even without hormonal stimulation (Li *et al.*, 2013). Furthermore, recurring rearrangements of the ER gene and its neighbouring gene have been linked to accelerated tumour growth and increased resistance to hormonal treatments (Robinson *et al.*, 2013; Tang *et al.*, 2016).

2.2.2 ATP-Binding Cassette Superfamily

The primary reason for the emergence of drug resistance in cancer is the proficient expulsion of anticancer drugs by cancer stem cells via Adenosine Triphosphate (ATP)-binding cassette (ABC) transporters (Zintle *et al.*, 2019). The members of the ABC superfamily are known to transport various substrates across the membrane. They play a role in the development of multidrug resistance in various cells. Numerous ABC proteins in humans function as efflux transporters. However, three specific ones – MDR1/P-glycoprotein (P-gp) (encoded by *ABCB1* gene), multidrug resistance protein 1 (MRP1) (encoded by *ABCC1* gene), and breast cancer resistance protein (BCRP) (encoded by *ABCG2* gene) - have been identified as the primary efflux

transporters responsible for multidrug resistance in cancer cells (Mao & Unadkat, 2014). *ABCG2* is a type of resistance marker that can be used to determine the prognosis of cancer and drug bioavailability (Kunnumakkara *et al.*, 2017; He *et al.*, 2018).

ATP-dependent P-gp is a factor in developing cancer resistance (Tuorkey, 2014). Although normal human breast tissue expresses P-gp to a limited extent, this protein is widely expressed in other normal human organs, safeguarding them from xenobiotics (Hutson *et al.*, 2010). MRP1 can capture and expel drugs in and outside the cell, while P-gp only works as a drug efflux pump in the cell membrane (Tang *et al.*, 2016). The protein BCRP has received the most attention in research, likely because it is the only member of the family that has been verified to induce the development of MDR in cancer (Kerr *et al.*, 2011). The discovery of BCRP occurred during the examination of breast cancer through the MCF-7 cell line (Tang *et al.*, 2016). Similar to P-gp/MRP1, the primary role of BCRP is to protect organs from foreign substances and harmful toxins. However, BCRP displays a greater level of adaptability compared to P-gp/MRP1, as it can transport hydrophilic and hydrophobic substrates (Jani *et al.*, 2014).

ATP-binding cassette transporters are responsible for carrying out the excessive efflux of drugs, which is one of the mechanisms that lead to drug resistance (Housman *et al.*, 2014). ATP-binding cassette transporters have two conserved cytoplasmic domains that bind ATP and two less conserved transmembrane domains. They release substrates across the cell membrane through ATP-driven energy (Wilkins, 2015). P-gp pumps drugs/toxins out of the cell using two ATP molecules. The presence of P-gp on cells prior to chemotherapy is considered intrinsic resistance

(Klopfleisch *et al.*, 2016). MDR1 and BCRP expression can cause drug resistance in tissues such as the lung, breast, and prostate, which do not naturally produce MDR (Housman *et al.*, 2014). MDR1 has a similar structure and function to P-gp, but it depends on glutathione (GSH) and only transports drugs modified by GSH (Keyvani-Ghamsari *et al.*, 2020). As a result, MDR1 plays a role in the timing of drug metabolism activation.

2.3 Nanotechnology Based Drug Delivery Systems

Manipulating materials at the nanoscale using nanotechnology results in creating versatile materials that find application in various fields of science and technology (Ganguly *et al.*, 2014). The surface of nanoparticles can undergo modification using diverse compounds, including ligands and drugs, to enable multifunctional therapy (Greineder *et al.*, 2016; Li *et al.*, 2016; Aftab *et al.*, 2018). The shape of nanoparticles has a significant influence on the absorption by cells and the effectiveness of anticancer agents (Kulkarni & Feng, 2013; Zheng & Yu, 2016; Aftab *et al.*, 2018). Nanoparticles have piqued considerable interest in biomedicine due to their unique properties, particularly in the delivery of cancer treatments. Nanotechnology-mediated drug delivery systems offer improved pharmacokinetics, such as higher clearance rates, greater distribution volumes, and increased bioavailability, facilitated by the enhanced permeability and retention (EPR) effect (Aftab *et al.*, 2018). The use of nanocarriers in formulation strategies is appealing due to their safe drug delivery, which protects against the harmful effects on non-target biological tissues and cellular structures (Zhang *et al.*, 2013; Aftab *et al.*, 2018). Another distinctive characteristic that makes nanoparticles attractive carriers for drug delivery is their ease of surface modification (Greineder *et al.*, 2016; Sohail *et al.*, 2016;

Aftab *et al.*, 2018). Choosing appropriate targets and nanocarriers is essential to minimise adverse reactions and improve the treatment efficacy against cancer cells. Achieving targeted drug delivery requires a comprehensive understanding of the nature of nanoparticles, drug properties, and their ability to release, cross biological barriers, and exhibit biocompatibility.

Nano-drug delivery offers advantages in overcoming obstacles associated with conventional drug delivery systems, such as poor drug absorption, low bioavailability, and inadequate biodistribution, which impede optimal clinical results (Xia *et al.*, 2014). Developing drug delivery systems capable of augmenting the pharmacological activity of drugs is crucial to mitigate these issues. In this context, nanomedicine offers the most effective approach as a targeted drug delivery system, avoiding any harmful impact on normal tissues while ensuring the desired drug levels in the bloodstream and tissues (Zhu *et al.*, 2013). The application of drug delivery systems has the potential to increase patient adherence, extend the lifespan of medications, and reduce healthcare expenses (Aminabhavi *et al.*, 2017). As a result, there is an increasing emphasis on creating precise and safe nanoparticle-based delivery systems for cancer treatment. These systems can be controlled and targeted to the affected area(s) (Man *et al.*, 2014; Sun *et al.*, 2014, 2016).

2.4 EPR Effect

The cut-off size for the vascular aperture in tumours ranges from 380-780 nm, and the arrangement of the vessels is influenced by factors such as the type of tumour, growth rate and microenvironment (Fang *et al.*, 2011; Aftab *et al.*, 2018). Drug delivery vectors ranging from 100-300 nm diffuse widely along vessels when extravasating, while 380-780 nm particles extravasate more centrally, indicating

varying vascular aperture cut-off sizes (Han *et al.*, 2016). Nanomedicines deliver drugs to target sites via extravasation, accumulating circulating nanoparticles mostly at the tumour site rather than normal tissues. In contrast to normal cells, tumour tissues have a longer retention time of drugs and nanoparticles attributed to the improper functioning of the lymphatic drainage system in tumour tissues (Yhee *et al.*, 2014). The EPR effect is the guiding principle for all nanocarriers to achieve selective accumulation of drugs and nanoparticles.

2.5 Drug Targeting

Drug targeting requires identifying the specific disease target and selecting an efficient drug carrier and proper route. The drug delivery system focuses on systemic circulation, using the body's natural response to target drugs based on physical and chemical properties. To improve patient outcomes and survival, therapeutic agents must selectively destroy targeted cells while avoiding damage to untargeted ones. This approach increases the concentration of the therapeutic agent while reducing toxicity and adverse reactions. Strategies such as active, passive, inverse, combination, and triggered targeting are employed to accomplish these goals effectively (Aftab *et al.*, 2018) (Figure 2.3). Passive targeting relies on the enhanced permeability and retention (EPR) effects, enabling nanocarriers to amass in tumour tissues via permeable blood vessels. Once these nanocarriers undergo modification with targeting ligands, they adhere to receptors on tumour cells, facilitating accurate drug delivery and internalisation (Shi *et al.*, 2023).

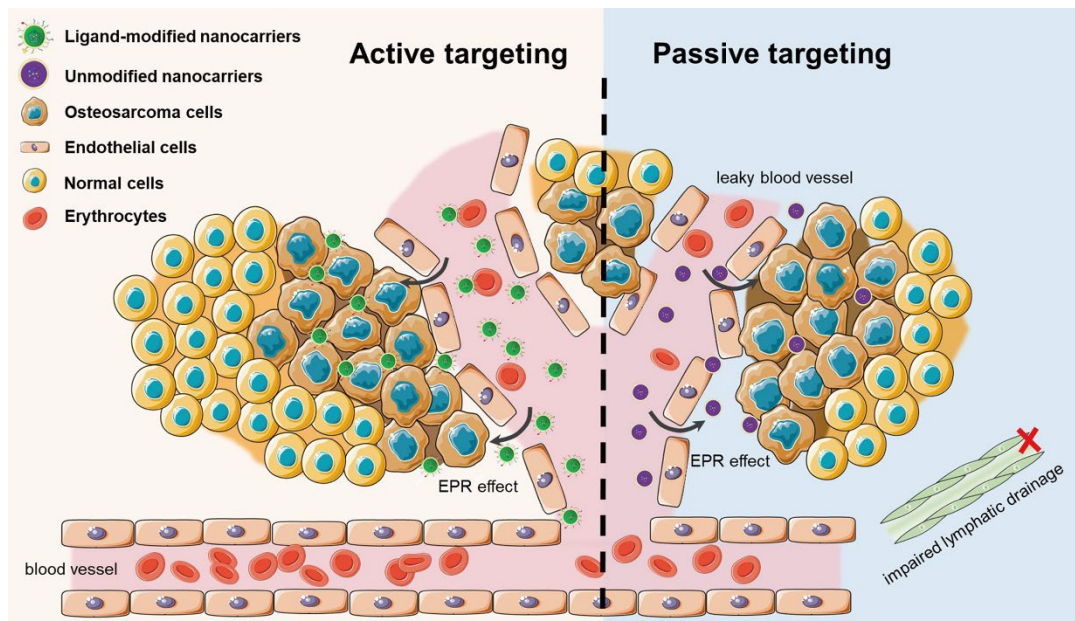


Figure 2.3: Targeting the tumour cells actively and passively assisted by the EPR effect. Adapted from Shi *et al.* (2023).

2.5.1 Passive Targeting

Passive targeting is limited by its reliance on the vascularisation of tumours and the process of angiogenesis. Nanoparticle release relies on tumour nature and is affected by interstitial fluid pressure, which is higher in tumours due to abnormalities in vessels and a disorganised lymphatic drainage system. The size of nanoparticles is crucial for accessing cancer cells, as the physiochemical characteristics of nanoparticles affect EPR-mediated targeting. Nanoparticles exceeding 100 nm tend to accumulate in the tumour microenvironment, whereas smaller nanoparticles can diffuse (Duan & Li, 2013). More suitable nanocarriers have been developed to address the effectiveness variability of nanoparticles in targeting tumours due to differences in tumour blood vessel structure. These nanocarriers have improved selectivity towards targeted cell uptake of nanoparticles. Passive targeting utilises the advantageous characteristics of tumour biology to facilitate the release of therapeutics into tumour cells through the EPR effect. The two common features of tumour cells are faulty lymphatic drainage and permeable blood vessels (Aftab *et al.*, 2018). The induction of

vascular factors such as angiogenesis and cytokines can lead to increased tumour vascular permeability, causing leakiness. Angiogenesis in tumours is marked by irregularly sized and shaped vascular organs, including arteries, capillaries and venules (Chen & Kaji, 2017).

2.5.2 Active Targeting

Active targeting refers to drug delivery to a specific site rather than being absorbed by the reticuloendothelial system (RES) (Schleich *et al.*, 2014; Aftab *et al.*, 2018). The concept of dual targeting relates to a carrier's ability to enhance the pharmacological potency of a drug and exert its therapeutic activity. Inverse targeting stops the RES from passively absorbing nanoparticles (Muro, 2012). The transportation of nanocarriers to the site of infection depends on blood circulation when administered into the bloodstream (Bae & Park, 2011). Selecting a targeting mechanism for drug delivery systems does not impact the number of nanoparticles that reach the tumour site. Passive and active targeting techniques are combined, with active targeting employed after passive accumulation in tumour cells has occurred (Torchilin, 2010; Chaturvedi *et al.*, 2013; Aftab *et al.*, 2018). Active targeting involves ligands and receptors designed to bind specifically to molecular targets on the surface of cells or tissues, enabling the delivery of drugs to particular organs or tissues via nanocarriers. These ligands are selected based on their higher expression levels in tumour cells than in normal cells, which enables them to bind with the receptors specifically (Aftab *et al.*, 2018). Nanoparticle surfaces have been modified using a range of ligands, including antibodies, aptamers, carbohydrates, vitamins, and peptides (Li *et al.*, 2014; Park *et al.*, 2014; Wang *et al.*, 2014; Xu *et al.*, 2014; Zhong *et al.*, 2014; Hudlikar *et al.*, 2016). Nanocarriers that are attached with ligands are internalised by target cancer cells through receptor-mediated endocytosis for drug

delivery (Behzadi *et al.*, 2017). This targeted delivery system minimises the side effects of drugs on healthy tissues by enabling the delivery of high drug concentrations to specific sites using lower dosages. Nanocarriers for drug delivery have been developed using a variety of polymers, including polysaccharides, poly(lactic-co-glycolic acid) (PLGA), proteins, and others (Kulkarni *et al.*, 2010; Aftab *et al.*, 2018). The desired therapeutic objectives determine the selection of polymers for nanocarriers. Polyethylene glycol (PEG) is commonly used to improve stability, but long-term use is limited due to oxidative impairment (Cole *et al.*, 2011; Jokerst *et al.*, 2011; Aftab *et al.*, 2018). PLGA and polylactic acid (PLA) are widely used in drug delivery as they can be hydrolysed to produce low-toxicity metabolites that can be eliminated via the Krebs cycle (Danhier *et al.*, 2012). The US Food and Drug Administration (FDA) recommends their use in therapeutic delivery.

2.6 Polymeric Nanoparticles

Polymeric nanoparticles aim to control drug release, improve tissue and cell compatibility, enhance intracellular uptake, stabilise active substances, and target specific tissues in drug delivery (Kumar *et al.*, 2017; Hernández-Giottonini *et al.*, 2020). Polymeric nanoparticles need a big size to impede quick entry into the bloodstream, yet small enough to avoid immune system clearance for optimal effectiveness (Robertson *et al.*, 2016). Although larger formulations have a higher potential for drug entrapment, it is essential to achieve a smaller nanoparticle size range to facilitate their ability to surmount biological obstacles and arrive at the location of the disease. Polymer-based nanoparticles are submicron-sized particles made of polymers. They can entrap or adsorb a therapeutic agent within their matrix or onto their surface (Mahapatro & Singh, 2011). Entrapping drugs in a nanocarrier

can enhance solubility and stability, potentially enabling the re-evaluation of drugs with poor pharmacokinetics (Dinarvand *et al.*, 2011).

2.6.1 Alginate-Based Nanoformulations

Alginate-based nanoparticles are extensively researched for drug delivery due to their biodegradability, biocompatibility, non-toxicity, and mucoadhesive properties (Chia *et al.*, 2022). Alginate is a hydrophilic polysaccharide that is linear in structure and consists of blocks of monomers (Figure 2.4). These monomers alternate between α -L-guluronic acid (G block) and β -D-mannuronic acid (M block) (Nayak *et al.*, 2020).

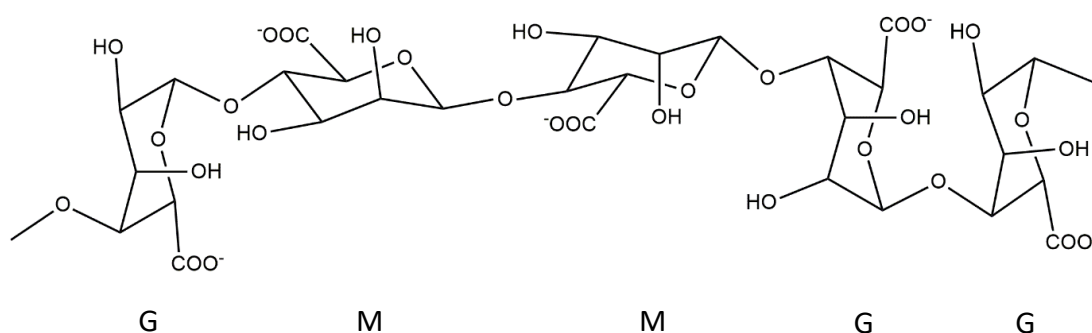


Figure 2.4: Structure of alginate.

The M block sections observe a flexible and linear structure, whereas the G block sections exhibit rigid and folded structures because the carboxyl groups experience steric hindrance (Sellimi *et al.*, 2015). Alginate with a high proportion of GG blocks has a greater solubility in water than that with a high proportion of MM blocks (Liu *et al.*, 2019). According to a former research done by Costa *et al.* (2018) stated that guluronic acid-rich films (M/G ratio of 30/70) demonstrated higher solubility than mannuronic acid-rich films (M/G ratio of 65/35) crosslinked with the same calcium chloride concentrations. This indicates that a higher concentration of calcium ion is needed for alginate structures with more G to achieve comparable solubility to films formed with low G content alginate. Additionally, the higher